EVOLUTION OF PARAMETERS AND INVESTIGATION OF PHENOMENA BY SIMULATING THE SUPERCHARGING OF A VW DIESEL ENGINE WHEN USING AN ELECTRICALLY DRIVEN AXIAL COMPRESSOR

Andrei – Cristian Grădinariu[1], Ioan Mihai [1]

[1]*Departament of Mechanical Engineering, Stefan cel Mare University of Suceava, Romania*
13 University Street, 720229, Romania, email: gradinariu_andrei@ymail.com

Abstract: *Supercharging of internal combustion engines is widely used in recent times. In this article we will present the results obtained by simulation in the ANSYS Academic programming environment for a VW diesel engine code ALH. The use of an axial compressor for supercharging the diesel engine is a new concept also due to the electric drive mode. This concept is distinguished by the fact that each compression stage consists of two rows of rotating vanes, which rotate in the opposite direction. Thus, the CFD simulation shows that this new concept determines the increase of the thermodynamic and kinematic parameters.*

Keywords: *bi-rotor axial compressor, simulation, supercharger, electric driven axial compressor*.

1. Introduction

The main objective of this article is to contribute to simulate the processes for a supercharging system based on an axial compressor with electrically driven double rotor. The study also presents the measurement of the performance of the electrically operated axial compressor performed by the author. The study continues with the realization of the mathematical model regarding the global calculation of the axial compressor, determining the thermodynamic parameters, kinematic and geometric parameters. Using the input data and running the ANSYS simulation software, a report is obtained with results for thermodynamic parameters such as fluid pressure and temperature and kinematic parameters such as overall speed, axial speed, and working fluid turbulence. By implementing this innovative supercharging system – Figure 1, real improvements can be made on the performance of supercharged engines. The supercharging system designed by [Mihai,2016] and shown in Figs. 1,2 eliminates some of the disadvantages of a conventional supercharging system. It is noted that the proposed idea is based on an electrically driven bi-rotor axial compressor, independent of engine speed.

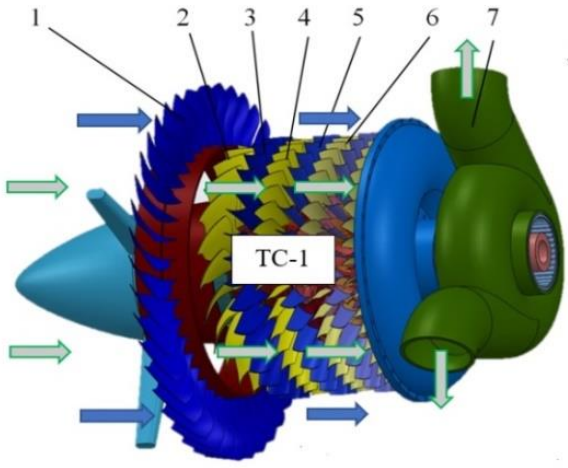

Figure 1: *Air flow through the compression stages of the TC-1 section for supercharging the engine, [Ansys,2020].*

The significance of the notations in Fig. 1, is: 1 - rotating vanes, acting as a turbo-fan, 2,3 – first stage of the axial compressor, 4,5 – second stage, 6 – third stage, 7 – outlet for the working fluid.

As can be seen from Fig. 1, the axial compressor is designed to generate two air jets:

- the first one is for cooling the engine with rotating vanes – 1, that acting as a turbo-fan,
- the second jet is the compressed air after sections TC-1 and TC-2 of the bi-rotor axial compressor where the movement of the blades is ensured by the electric motors rotating in the opposite direction.

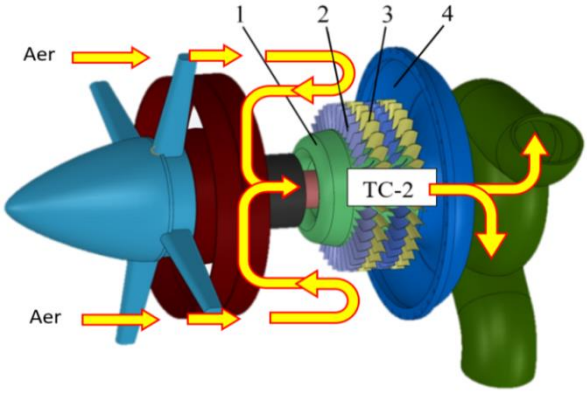

Figure 2: *Air flow through the compression stages of the TC-2 section for supercharging the engine [Ansys,2020].*

The increase of the air flow necessary for the supercharging system is achieved by the entry of the working fluid in the five compression stages from section TC-1 – Fig. 1. The TC-2 section – Fig. 2 of the axial compressor consist other 2 stages. The rotating vanes – 2,3 are driven in the opposite direction by electric motors. The air will enter the first compression stage of the TC-2, being directed at the exit of the blades to a new compression stage.

Since the compression stages are double rotor (without stator blades) the parameters will be significantly higher than the classic case of an axial compressor due to the doubling of the peripheral speeds in the speed triangle. It should be noted that after returning the compressed air to 180 degrees the air flow from the first TC-1 compression section passes to the second TC-2 section. This is ensured by the semithoroidal channel 4 which also has a cooling role of the working agent.

2. Simulation methodology

The purpose of simulating in the CFD environment the processes that occurs during the operation of the axial compressor is to represent and explain the evolution of thermodynamic and kinematic parameters. The axial compressor proposed for simulation is the concept developed by the author [1]. The evolution of the parameters is followed, such as: *the increase of the temperature and the pressure* of the working fluid in those five compression stages, *the evolution of the air density*, *the intensity of the turbulences* that appear when the blades rotate, or the *axial speed*.

2.1 The mathematical model for the global calculation of the axial compressor

The solution chosen for the axial compressor is with *a constant tip diameter* and *a variable base diameter*, which is easily seen from a constructive point of view in Fig. 3. In order to perform the global calculation of the axial compressor, Fig. 4 shows the plan unfolding of a compressor stage with the corresponding speed triangles.

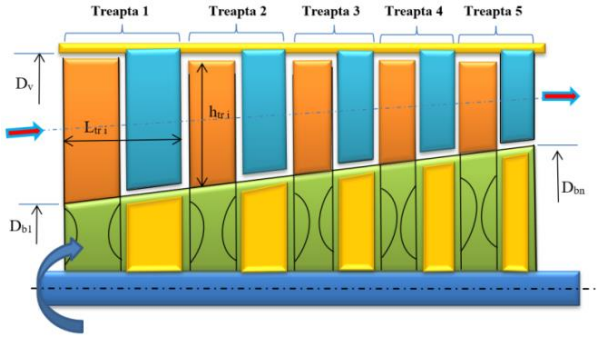

Figure 3: *Air circulation through section of the axial compressor.*

The theoretical area of the air inlet to the compressor, for the first compression stage takes into account the value of the ratio between fluid velocity and critical velocity. It is called the velocity coefficient, but is also the linear dependence between air flow and mechanical work consumed.

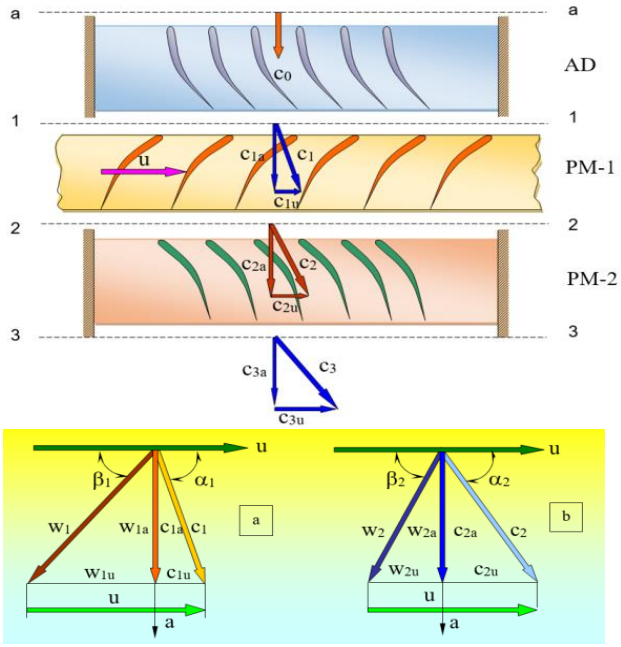

Figure 4: *The triangle of velocities in a compression stage, after [Pimsner,1986], [Pimsner,1988], [Nagpurwala,2019]*

Theoretical area at the air inlet to the compressor is determined by Eqs. (1, 2):

$$A_{i,1} = \frac{P_c\ \eta_c \sqrt{T_{1,i}}}{0,04\ i_{1,i}\left(\pi_c^{\frac{k_a-1}{k_a}} - 1\right) p_1\ \lambda_{1m}\ \sin\alpha_{1,i}} \tag{1}$$

$$\text{unde}\ \ \lambda_{1m} = \frac{c_{1i}}{\sqrt{2\frac{k_a-1}{k_a+1} i_{1,i}}}\left[m^2\right]$$

Using as a simplifying hypothesis that in the axial direction the absolute velocity component is conserved, the area at the outlet of the working fluid can be calculated with Eg. (2).

$$A_{e,2} = \frac{P_c\ \eta_c \sqrt{T_{2,e}}}{0,04\ i_{2,e}\left(\pi_c^{\frac{k_a-1}{k_a}} - 1\right) p_{2,e}\ \lambda_{2a} \sin\left(\alpha_{2,e}\right)} \tag{2}$$

$$\text{unde}\ \ \lambda_{2e} = \frac{c_{2e}}{\sqrt{2\frac{k_a-1}{k_a+1} i_{2,e}}}\ [m^2]$$

In this article it will be presented the mathematical model for the first compression stage, due to the large calculation volume. Thus the equations of the thermodynamic, kinematic and geometric parameters of the two-flow axial compressor are presented below [Pimsner,1986], [Pimsner, 1988], [Stanciu, 2008].

1. Thermodynamic parameters for stage I:

$$S_{TI}\begin{cases} T_{12}(n_c) = T_1 + \dfrac{\left(i_1 + l_{tr1}(n_c)\right) - \dfrac{c_{2u}^2}{2}}{c_p}\ [K] \\ \pi_{tr12}(n_c) = \left(1 + \dfrac{l_{tr2}(n_c)\,\eta_{tr}}{i_1}\right)^{\frac{k_a}{k_a-1}} \\ p_{12} = p_1\ \pi_{tr}(n_c),\ [Pa] \end{cases} \tag{3}$$

2. Kinematic parameters for stage I:

$$S_{CI}\begin{cases} u_{m12} = \dfrac{1}{2} u_{1v}(n_c)\left(1 + \dfrac{D_{1b}}{D_{1v}}\right),\ \left[\dfrac{m}{s}\right]. \\ c_{u12} = \left(1-\rho_{12}\right) u_{1m}(n_c) - \dfrac{l_{tr1}(n_c)}{2\,u_{1m}(n_c)},\ \left[\dfrac{m}{s}\right] \\ c_{a12} = \dfrac{\dot{M}_a}{\rho_a A_i}\left[\dfrac{m}{s}\right] \\ c_{12}(n_c) = \sqrt{c_{a12}^2 + c_{u12}^2(n_c)},\ \left[\dfrac{m}{s}\right] \\ \lambda_{12}(n_c) = \dfrac{c_{12}(n_c)}{\sqrt{2\dfrac{k_a-1}{k_a+1} i_{12}}} \dfrac{1}{100} \\ q_{\lambda_{12}}(n_c) = \lambda_{12}(n_c)\left[\dfrac{k_a+1}{2}\left(1 - \dfrac{k_a-1}{k_a+1}\lambda_{12}(n_c)\right)\right]^{\frac{1}{k_a-1}} \end{cases} \tag{4}$$

3. Geometric parameters for stage I:

$$S_{GI}\begin{cases} A_{12}(n_{\min}) = \dfrac{M_a \sqrt{T_{12}}}{0,004\, q_{\lambda_{12}}\ p_{12} \sin\alpha_{12}}\left[m^2\right] \\ D_{b12}(n_{\min}) = \sqrt{D_{1v}^2 - \dfrac{4\,A_{12}(n_{\min})}{\pi}}\ [m] \\ h_1(n_{\min}) = \dfrac{D_{1v} - D_{12b}(n_{\min})}{2}[m] \\ L_{tr1} = \dfrac{h_1}{-(3-4,5) - (1-2)\dfrac{i-1}{z-1}}[m] \end{cases} \tag{5}$$

where: P_c = *1.5[kW]* - power received at the shaft, π_c = 1.7 - axial compressor compression ratio, π_{tr12} – compression ratio of the first compression stage, η_c = *0,88[%]* -

compressor efficiency, $T_1 = 288{,}15$ [K] – inlet air temperature, T_{12} - air temperature after stage, i – enthalpy [J], l - Specific mechanical work [J/kg], n_c - compressor speed [r.p.m], c_u – absolute speed components [m/s], c_p - specific heat [J/kg K], η_{tr} - compression stage efficiency, $k_a = 1{,}4$ - adiabatic exponent, $p_1 = 0.93392 \cdot 10^5$ [Pa] - inlet fluid pressure, p_{12} - air pressure after stage I, u_{m12} - tangential velocity component for stage I [m/s], c_{u12} - tangential direction velocity component for stage I [m/s], c_{a12} - absolute speed for stage I [m/s], u_1 - tangential velocity component [m/s], D_b - diameter at the base [m], D_v - diameter at the tip, A_{12} - surface area for stage I, h_1 - step height [m], L - stage length [m], ρ - compression stage coefficient, $\dot{M}$ - mass intake air intake [m/s], ρ_a - air density [kg/m^3], $q(\lambda) = 0.3455$ - speed coefficient.

2.2 The evolution of the parameters in the five compression stages of the axial compressor

Figure 5 and Figure 6 shows the variation of the air temperature on each compression stage determined using the mathematical model in Mathcad [Hendrick,1986], [Pimsner,1986], [Pimsner,1988], [Stanciu,2008], [Socaciu,2017], .

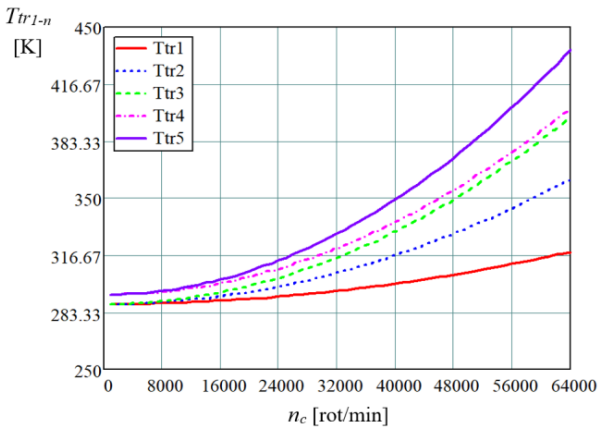

Figure 5: *The evolution of the temperature with the speed in each stage of the axial compressor.*

Analyzing the analytically calculated results from Fig. 5, it is observed that at the maximum speed of the axial compressor, the highest temperature value is 436.38 [K] for the 5th stage, which shows an increase of 51.43% compared to the first stage.

It is known that a slight depression occurs when entering the compressor. From the calculations in Fig. 6 it is found that at the exit of the last stage of the axial compressor the maximum value of the boost pressure is reached $p_c = 3.082 \cdot 10^5$ [Pa].

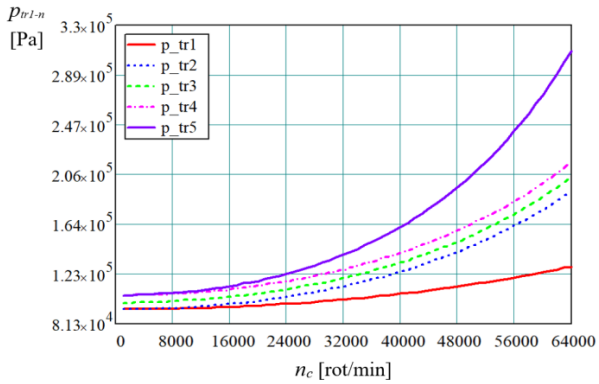

Figure 6: *The evolution of the boost pressure with the speed in each stage of the axial compressor.*

The values obtained in Fig. 7, show us that there are no very large differences between the tangential speeds in the axial compressor blades.

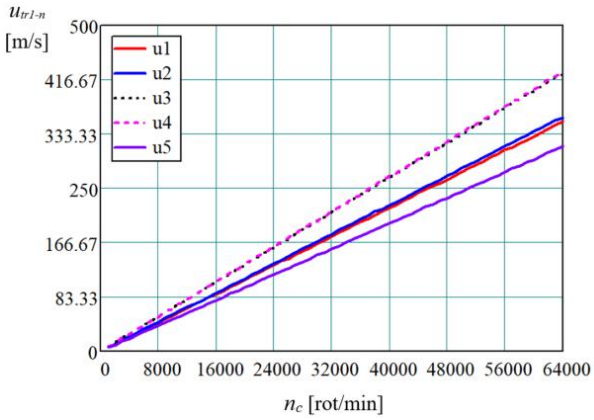

Figure 7: *Tangential speed for the 5 compression stages*

Regardless of the number of stages, at speeds up to 15.000[r.p.m.] lower speeds are reached but from the calculations it results that at the maximum speed of 64.000[r.p.m.] sonic or supersonic speeds can be reached. However, the calculations do not take into account the losses due to friction and ventilation, which are much higher at such high speeds.

According to the obtained results, the linear variations in Fig. 8 highlight the fact that for the peripheral component of the absolute velocity of the fluid there is an increase given the increase of the speed.

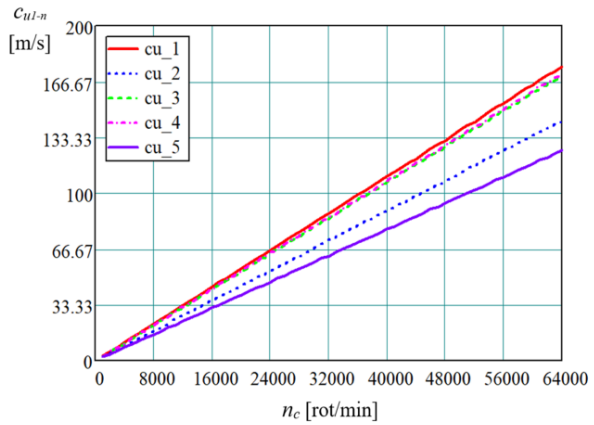

Figure 8: *Peripheral component of the absolute speed for the 5 compression stages*

The velocity increases linearly to a maximum value with c_{12}=175.89[m/s]. According to the data obtained – Fig. 9, the highest value of the absolute speed is obtained for the maximum speed in stage 1 when c_{11}=233.58 [m/s] speed which is 51.96% higher than that in the 5th stage.

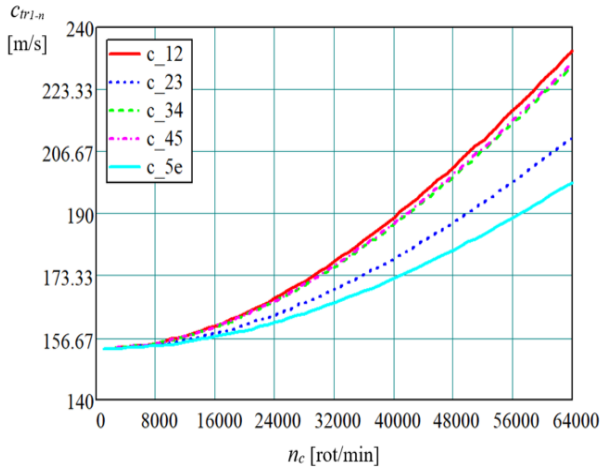

Figure 9: *Absolute speed for the 5 compression stages*

It is found that the sonic speed is not reached in either the previous case or in this one. The figure shows that c_{12} shows an increase of 34.6% from minimum to maximum speed.

2.3 Setup simulation for Ansys 2020

The Ansys 2020 academic simulation medium was used to analyze the characteristic parameters of the axial compressor [Ansys,2020].

The simulation in ANSYS CFD involves several steps:

- definition of the type of compressor and the axis of rotation of the components;
- adding components and defining them: rotor 1 / rotor 2;
- introduction of the number of rotations in the case of rotor components;
- defining the inlet parameters: working fluid type, reference pressure, inlet pressure and temperature, maximum pressure at the compressor outlet;
- definition of expressions - relations of simulation, storage of variables, etc .;
- running simulations with the CFX-Solver Manager extension.

To perform the simulations, we opted for the construction variant known as constant peak diameter and variable base diameter.

Based on the simplified assumptions imposed, the ideal gas was chosen as the working fluid. Simulation of turbulence occurring in the working fluid can be performed by two methods:

- the method k - ϵ which characterizes the most common turbulence model in the dynamic calculation of fluids, where k represents the kinetic energy of the turbulent motion and ϵ is the degree of dissipation of the kinetic energy of turbulence [Okey,1995].
- the Shear Stress Transport method (k - ω) which describes a turbulence model using two partial differential equations for two variables: *k* is the kinetic energy of the turbulent motion and *ω* is the rate of dissipation of the turbulent kinetic energy from the internal thermal energy [David,2008], [Georgiadis,2013].

In this case, the turbulence model (k - ω) was chosen, which is based on the Eqs. (6,7):

$$\frac{\partial(\rho k)}{\partial t}+\frac{\partial\left(\rho u_j k\right)}{\partial x_j}=\rho\tau_{ij}\frac{\partial u_i}{\partial x_j}- \\ -\beta^*\rho\omega k+\left[\left(\mu+\sigma_k\frac{\rho k}{\omega}\right)\frac{\partial k}{\partial x_j}\right] \quad (6)$$

$$\frac{\partial(\rho\omega)}{\partial t}+\frac{\partial(\rho u_j\omega)}{\partial x_j}=\frac{\alpha\omega}{k}\tau_{ij}\frac{\partial u_i}{\partial x_j}-\beta\rho\omega^2+ \\ +\frac{\partial}{\partial x_j}\left[\left(\mu+\sigma_\omega\frac{\rho k}{\omega}\right)\frac{\partial\omega}{\partial x_j}\right]+\frac{\rho\sigma_d}{\omega}\frac{\partial k}{\partial x_j}\frac{\partial\omega}{\partial x_j} \quad (7)$$

3. Results obtained by simulating the processes of an electrically driven axial compressor

The graphs in Figs. 10 - 12 represent the variation of the air turbulence intensity in the compression process, from the first 3 compression stages that form the TC1 section of the axial compressor.

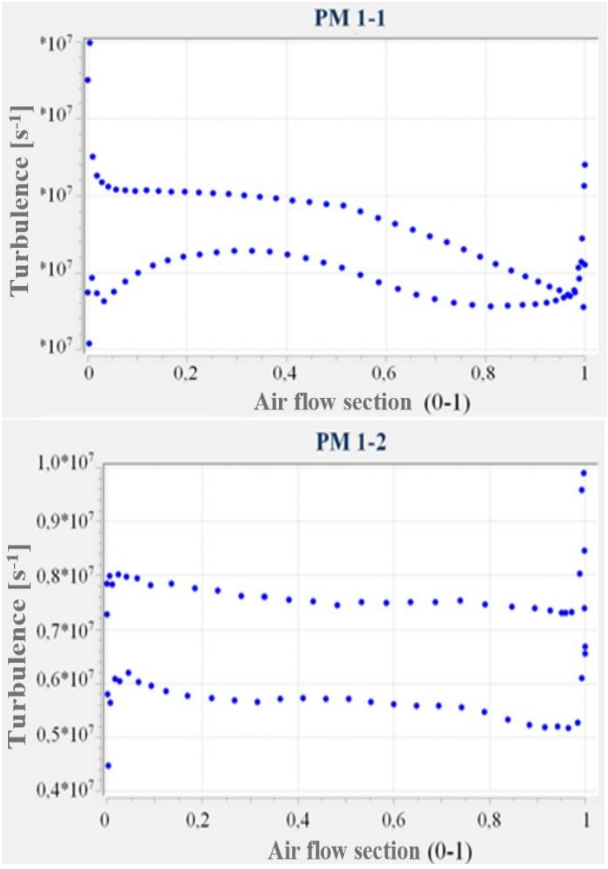

Figure 10: *The evolution of air turbulence intensity in stage I.*

It is known that we have a turbulent flow if the air flow regime is characterized by stochastic fluctuations of the properties.

The intensity of air turbulence is characterized by the degree of formation of turbulent kinetic energy, more precisely by the speed with which energy is transferred to the air flow [Okey, 1995], [David, 2008], [Georgiadis, 2013], [Simelane, 2015].

Following the evolution of the turbulence on the area of the soffit and extrados of the pallets in Fig. 10, it is clearly observed that the turbulence is much higher in the PM1-1 mobile pallet network and almost constant in PM1-2. The lowest value of turbulence intensity obtained by simulation is in PM1-2, $\epsilon = 0.57\cdot10^7$[s-1] and the maximum value in PM1-1 is $\epsilon=2.17\cdot10^7[s^{-1}]$.

Following in Fig. 11 the evolution of turbulence on the area of the soffit and extrados of the pallets and based on the values obtained it is easily observed that the turbulence is much higher in the PM2-1 mobile pallet network remaining almost constant on the soffit and extrados pallets at $\epsilon_{PM2\text{-}1}=0.06\cdot10^9$ [s^{-1}].

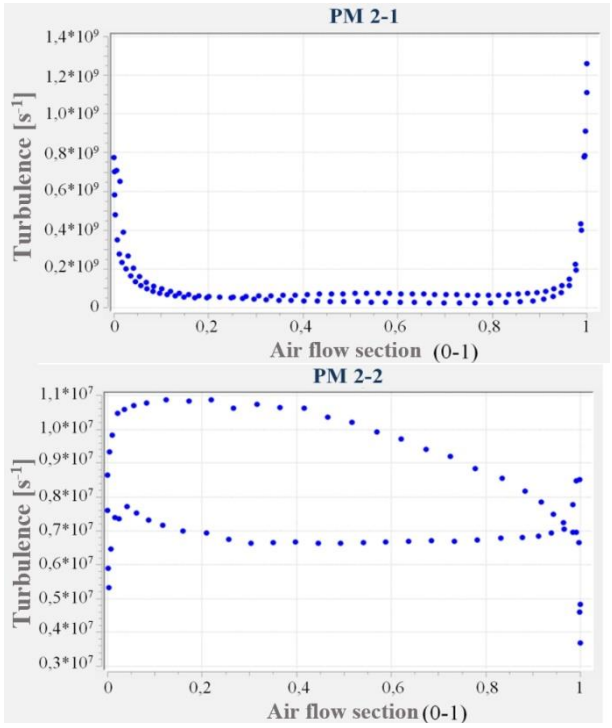

Figure 11: *The evolution of the air turbulence intensity in the second stage.*

The value of turbulence intensity obtained by simulation for the PM2-2 mobile pallet network has values between $\epsilon_{PM2-2}=(0.63\div1.08)\cdot10^{7}[s^{-1}]$.

Analyzing the data obtained in Fig. 12 it is noticed that the turbulence intensity remains almost constant on the soffit and extrados of the PM3-1 network blades at values between $\epsilon_{PM3-1}=(0.044 \div 0.12)\cdot10^{8}[s^{-1}]$.

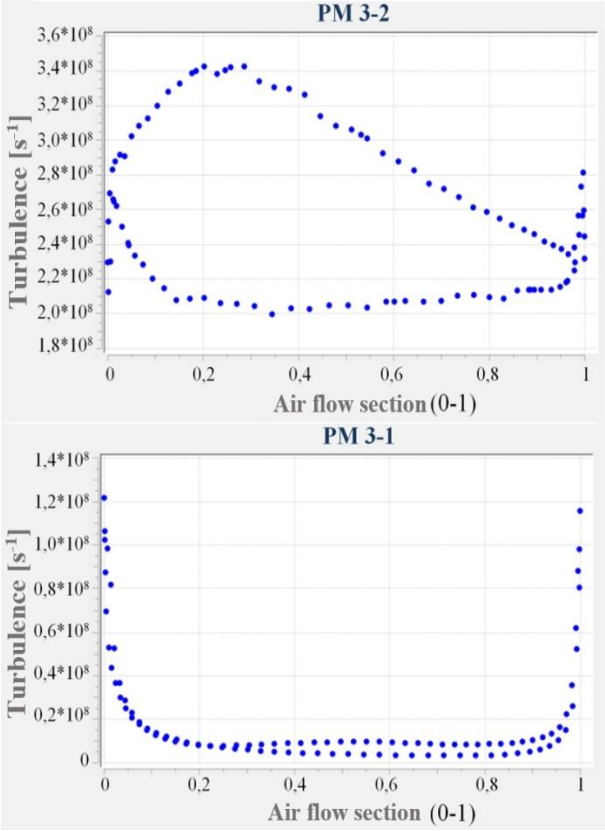

Figure 12: *The evolution of the air turbulence intensity in the third stage.*

On the other hand, regarding the evolution of the turbulence intensity in the PM3-2 vane network, it is found that the values are higher and are in the range:

$\epsilon_{PM3-2}=(2.05 \div 3.38)\cdot10^{8}[s^{-1}]$.

Following the performed simulations, a global vector analysis can be performed for the parameters of the first TC-1 compression section.

Figure 13 shows the evolution of static pressure.

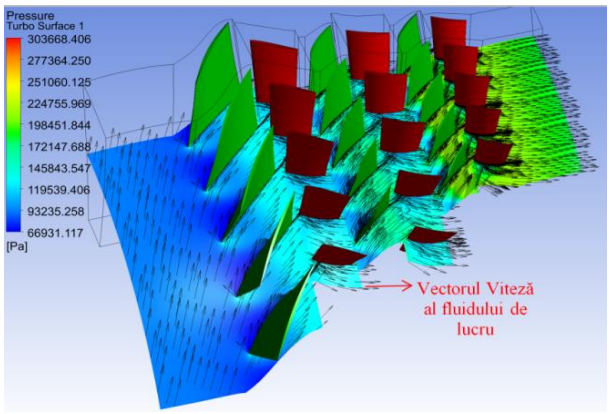

Figure 13: *Evolution of static pressure in TC-1.*

This parameter referring to the internal pressure in TC-1 reaches values in the range $p_{st}=0.7\div2.18\cdot10^{5}$ [Pa] between the air inlet and outlet of the movable blades of the axial compressor. Figure 14 shows the evolution of the total pressure.

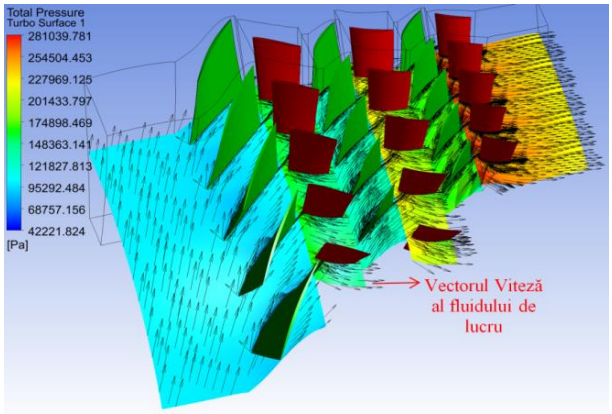

Figure 14: *Evolution of total pressure in TC-1.*

The simulation shows the advantage of the proposed constructive solution by observing an increase of the total pressure and the velocity vector towards the exit from the PM3-2 moving vanes where a maximum value that can reach $p_{din}=2.5\div2.8\cdot10^{5}$[Pa] is reached.

Figure 15 represents the temperature evolution for the case of simulating the static pressure of the working fluid. According to the scale in the figure, the following temperature values are recorded: stage I: $T_{trI}=290\div310$[K], stage II: $T_{trII}=310\div320$[K], stage III: $T_{trIII}=320\div350$[K]. Figure 15 shows the evolution of the total temperature (for the case of simulation in the case of the total flow pressure of the working agent) which actually shows how the kinetic energy is changed into

internal energy expressed by temperature variation.

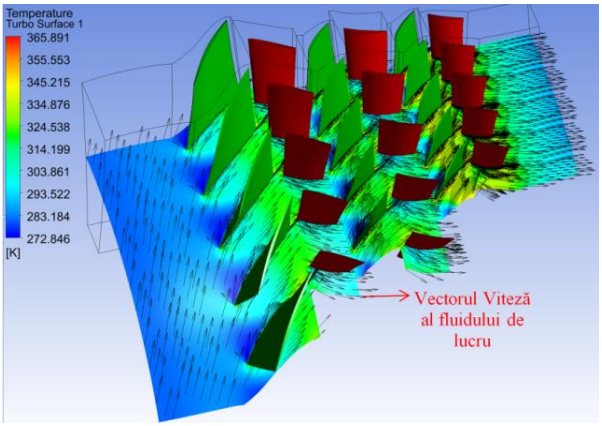

Figure 15: *The evolution of the stagnation temperature in TC-1.*

In PM1-2 the total temperature is maintained at T_{PM1-2}=300÷330[K], then it increases progressively so that at PM3-2 it reaches a maximum of $T_{PM3-2max}$=360[K].

According to the results obtained by simulation from Fig. 16 it can be seen that the air density oscillates on the TC-1 steps between ρ_{ac}=0.72÷2.33[kg/m3].

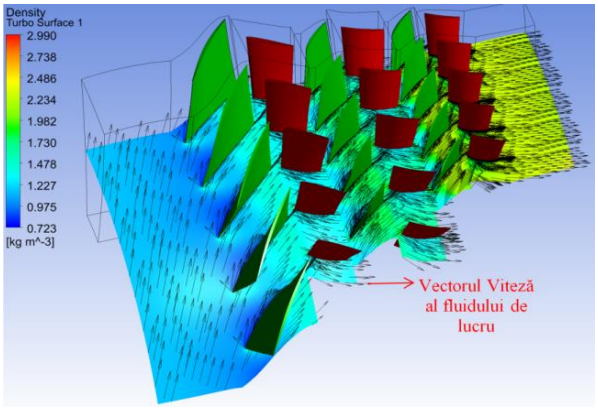

Figure 16: *Evolution of air density in the TC-1*

The axial speed – Fig. 17 has a continuous increase from the air intake to its exhaust, starting from a minimum $c_{PM1-1min}$=75.91[m/s] in PM1-1, reaches in the second stage a value c_{PM2-2}=210 [m/s] and leaves TC-1 with c_{PM3-2}=180[m/s].

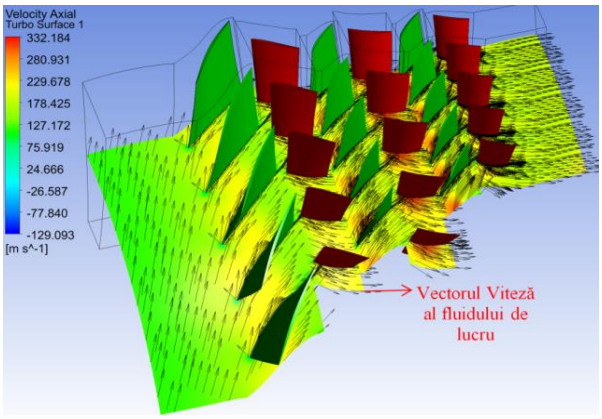

Figure 17: *Axial speed variation in TC-1 section*

4. Conclusions

Following the test results and the simulation in the CFD environment, the following conclusions were drawn:

1. Measurements made on the axial compressor show that at a speed of the electrically driven axial compressor n_{CAx}=18.000[r.p.m] (1/3 of the maximum speed) the supercharger repels a mass flow $m_{1/3}$=0.013[kg/s].
2. The same test stand shows that increasing the compressor speed to n_{CAx}=36.000[r.p.m] leads to a flow $m_{2/3}$=0.021[kg/s].
3. The axial compressor represses a maximum mass flow m_{max}=0.032[kg/s], at a speed n_{CAx}=54.000[r.p.m].
4. From the measurements made it appears that the maximum pressure made by the axial compressor is $p_{CAx}=1.81\cdot10^5$[Pa]. The result is close to the value of the turbocharger at the factory, but it should be noted that an axial compressor with only two compression stages was used.
5. The simulation in the CFD environment for an axial compressor with five compression stages shows a maximum boost pressure $p_{CAx} = 3.082\cdot10^5$[Pa].
6. For the diesel engine equipped with an axial compressor driven at a maximum speed of n_{CAx}=54.000[r.p.m], the data show that the power of the VW ALH diesel engine reaches a maximum value $P_{CAx100\%}$=45.52[kW] at an engine speed

$n_{PCAx100\%}$=3864.32[r.p.m]. The value show an increase of 21.99% over the naturally aspirated engine and 10.53% over the first test with the speed of axial compressor n_{CAx}=18.000[r.p.m].

7. The maximum available torque $M_{CAx100\%}$=137.49[Nm] at engine speed $n_{MCAx100\%}$ = 1894.09[r.p.m.] is 13.71% higher than the naturally aspirated engine and 12% higher than the first axial compressor test.

References

1. [Mihai,2016] Mihai, I., Olariu, E., *Biflow axial compressor, has air flows for external cooling and supercharging of internal combustion engines*, Derwent Innovations Index Web of Science - Primary Accession Number: 2013-N13039, Patent Number(s): RO128769 B1 from 30.06.2016.
2. [Nagpurwala,2019] Nagpurwala Q.H., *Introduction to turbomachines, Axial Compressors, Presentation*, M.S. Ramaiah School of Advanced Studies, pp. 1-72, 2019.
3. [Okey,1995] Okey K., Forrest A., *Advanced k-ϵ modeling of heat transfer*, NASA Contractor Report 4679, No. NAS3 – 25950, pp. 157, 1995.
4. [Pimsner,1988] Pimsner V., *Mașini cu palete – Procese și Caracteristici*, Ed. Tehnică București, 448 pag., 1988.
5. [Pimsner,1986] Pimsner V., Berbente C., ș.a., *Procese în mașini termice cu palete – Aplicații și probleme*, Ed. Tehnică București, 383 pag., 1986.
6. [Socaciu,2017] Socaciu L., Giurgiu O., *Termotehnică – sinteze lucrări de laborator, Lucrarea nr. 5*, Ed. UTPRESS Cluj Napoca, ISBN 978-606-737-227-4, 70 pag., 2017.
7. [Stanciu, 2008] Stanciu V. Stroe G., ș.a., [Compresoare cinetice aerodinamice], Ed. Printech București, ISBN 978-973-718-968-4, 336 pag., 2008.
8. [David,2008] David C.W., *Formulation of the k-ω – Turbulence Model Revisited*, Research Article in AIAA Journal, DOI: 10.2514/1.36541, pp. 16, 2008.
9. [Hendrick,1986] Hendrick P., [Turbomachinery course - Axial compressors], Ecole Polytechnique de Bruxelles, pp. 15,
10. [Georgiadis,2013] Georgiadis N. J., Yoder D. A., *Recalibration of the Shear Stress Transport Model to improve calculation of the Shock Separated Flows*, Research Article in 51st Aerospace Sciences Meeting, DOI: 10.2514/6.2013-685, pp. 30, 2013.
11. [Simelane,2015] Simelane P., [Axial-compressor and turbine design project for a Cessna 550 fighter-plane], Course: B. Tech Mechanical Engineering, University of Johannesburg, No. TUM411, pp. 28, 2015.